2007

Study of Soliton Stabilization in D+1 Dimensions using Novel Analytical and Numerical Techniques

George Nehmetallah
The Catholic University of America

Partha P. Banerjee
University of Dayton, pbanerjee1@udayton.edu

Research Signpost
37/661 (2), Fort P.O., Trivandrum-695 023, Kerala, India

Nonlinear Optics and Applications, 2007: 31-60 ISBN: 978-81-308-0173-5
Editors: Hossin A. Abdeldayem and Donald O. Frazier

2

Study of soliton stabilization in (D+1) dimensions using novel analytical and numerical techniques

G. Nehmetallah and P.P. Banerjee
Department of Electrical and Computer Engineering, University of Dayton, Dayton, OH 45469, USA

Summary

In this Chapter, we provide a brief review of the underlying nonlinear Schrödinger and associated equations that model spatio-temporal propagation in one and higher dimensions in a nonlinear dispersive environment. Particular attention is given to fast adaptive numerical techniques to solve such equations, and in the presence of dispersion and nonlinearity management, saturating nonlinearity and nonparaxiality. A unique variational approach is also outlined which

Correspondence/Reprint request: Dr. P.P. Banerjee, Department of Electrical and Computer Engineering University of Dayton, Dayton, OH 45469, USA. E-mail: partha.banerjee@notes.udayton.edu

helps in determining the ranges of nonlinearity and dispersion parameters to ensure stable solutions of the nonlinear equations. The propagation of 3+1 dimensional spatio-temporal pulses, or optical bullets is also modeled using a fast adaptive split-step Hankel transform technique.

1. Introduction

Traditionally, solitons or solitary waves propagating in a medium are caused by a balance between nonlinearity and dispersion. Mathematically, solitons are particular solutions of nonlinear partial differential equations modeling many physical phenomena. The soliton was first described by John Scott Russell in 1834, who observed a solitary wave in the Union Canal, reproduced the phenomenon in a wave tank, and named it the "Wave of Translation". In 1895, Korteweg and deVries mathematically described weakly nonlinear shallow water waves with an equation that later came to be known as the KdV equation [1,2,3]. Since then, this and similar equations have been found in a wide range of physical phenomena, especially those exhibiting shock waves, and traveling waves and solitons. In 1965 Zabusky and Kruskal used a finite difference approach to numerically solve the KdV equation and the word “soliton” was first used [2]. Rigorously speaking, the soliton is a special subset of solitary waves that is stable to perturbations and mutual collisions; however, the word is sometimes used loosely in the literature to denote stationary traveling wave solutions of nonlinear partial differential equations.

In nonlinear optics, solitons can be classified as temporal (1-dimension), spatial (1 and 2-dimensions) or spatiotemporal (3-dimensions) depending on whether the light is confined in time, space, or space and time, respectively. Hence a temporal soliton represents an optical pulse that does not change its shape while propagating in nonlinear media, such as a Kerr type medium. Similarly, a spatial soliton is a confined beam in direction(s) transverse to propagation. Temporal solitons in Kerr type media are formed due to the balance of two counter effects, viz., dispersion, which leads to pulse broadening, and self phase modulation (SPM) where the refractive index depends on the intensity of the pulse. Spatial solitons are formed due to the balance between beam diffraction which induces spreading of the beam, and the self focusing phenomena due to the Kerr nonlinearity. Spatiotemporal solitons or optical bullets exist due to the balance between dispersion, diffraction and Kerr nonlinearity effect.

During the last two decades there has been a lot of interest in optical solitons. Different kinds of solitons have been introduced, namely, Bragg, gap, vortex, parametric, discrete, algebraic, vector and incoherent solitons along with different “shades” associated with them, such as bright, dark and gray.

For a complete list of these the reader can refer to the book by Kivshar and Agrawal [4].

Chronologically, the first spatial soliton was discovered in 1964 due to the nonlinear phenomenon of self-trapping of continuous wave optical beams in a bulk nonlinear media [4]. In 1973, Hasegawa was the first to suggest the existence of temporal solitons in optical fibers, due to a balance between self-phase modulation and anomalous dispersion, and to propose the idea of a soliton-based transmission system to increase performance in optical telecommunications [5]. In 1980, Mollenauer *et al.* were the first to experimentally observe these temporal solitons [6, 7]. In 1987, Emplit *et al*. made the first experimental observation of the propagation of a dark soliton in an optical fiber [7]. In 1988, Mollenauer *et al*. used the Raman effect to transmit soliton pulses over 4,000 kilometers [8]. In 1991, Gordon *et al*. transmitted solitons error-free at 2.5 Gbps over more than 14,000 kilometers, using erbium optical fiber amplifiers [9]. In 1998, Georges *et al*. used wavelength division multiplexing through combining optical solitons of different wavelengths, and demonstrated data transmission of 1 Tbps [10]. In 2001, solitons became a practical reality when submarine telecommunications using solitons was first realized in Europe carrying real traffic [12].

2. Theoretical background

2.1 Pulse propagation in fiber: The 1-D NLS equation

It is well known that pulses traveling in a nonlinear medium distort due to the effect of nonlinearity. Also linear theory predicts that pulses distort due to dispersion that may exist in the medium. This phenomenon is due to the fact that different frequency components constituting the pulse travel with different velocities in a dispersive medium. So, it is surmised that nonlinearity and dispersion together can accommodate distortionless propagation of pulses, called solitons. For both nonlinearity and dispersion, chirping in frequency develops during propagation. Appropriate amounts of each ensures soliton-like propagation.

Fiber dispersion can be best understood by realizing that the propagation constant k is not a constant but depends on frequency according to the dispersion relation [13] $\mathrm{k}(\omega)=\mathrm{k}_0+(\omega-\omega_0)\mathrm{k}_1+\frac{1}{2}(\omega-\omega_0)^2\mathrm{k}_2+\frac{1}{6}(\omega-\omega_0)^3\mathrm{k}_3+\ldots$, where k_0 is the propagation constant at frequency ω_0, $k_1 = k'(\omega_0)$, is the group velocity (GV) parameter, $k_2 = k''(\omega_0)$ is the group velocity dispersion parameter (GVD), and $k_3 = k'''(\omega_0)$ is the slope of the group velocity.

An optical pulse with an envelope u_e propagating in a single mode fiber will have a spectral width $\Delta\omega$, since $n = n\left(\omega,|u_e|^2\right)$ depends on frequency. Then

$n_g = n_0 + \omega \dfrac{dn_0}{d\omega}$, where n_g is the group index. Hence, the pulse amplitude u_e travels at a group velocity $\upsilon_g = \dfrac{1}{k_1} = \dfrac{c}{n_g}$. Thus, different spectral components travel at different speeds along the fiber causing dispersion. This phenomenon is called GVD and is denoted by parameter $k_2 = k''(\omega_0)$, where $k_2 > 0$, (<0) corresponding to normal dispersion (ND) and anomalous dispersion (AD), respectively. We note that dispersion broadens the pulse shape.

The effect of the nonlinearity is manifested in the intensity dependence of the refractive index $n\left(\omega,|u_e|^2\right) = n_0 + n_2|u_e|^2 = n_0 - \dfrac{n_0\hat{\beta}_3}{2}|u_e|^2$, where $\hat{\beta}_3$ is responsible for self refraction [1,13]. The third order $\chi^{(3)}$ susceptibility, which is also related to n_2, is the nonlinearity present in optical fibers, and is responsible for nonlinear refraction. This phenomenon is called self phase modulation (SPM), where the optical pulse experiences spectral broadening or self-focusing in time domain. Note that one can use a heuristic method to derive the nonlinear Schrödinger (NLS) equation by using the dispersion relation and operator method as outlined in Refs. [1,13], to get:

$$j\frac{\partial u_e}{\partial T'} - \frac{\upsilon_g'}{2}\frac{\partial^2 u_e}{\partial Z'^2} + \frac{\omega_0\hat{\beta}_3}{4}|u_e|^2 u_e = 0, \tag{1}$$

which is the 1-D NLS equation. In (1), $\upsilon_g = \left.\dfrac{d\omega}{dk}\right|_{k_0}$, $\upsilon_g' = \left.\dfrac{d^2\omega}{dk^2}\right|_{k_0}$, $u(Z',T') = Re\left[u_e(Z',T')e^{j(\omega_0 T' - k_0 Z')}\right]$ is the optical field, and $a \approx |u_e|$, $\dfrac{\omega_0\hat{\beta}_3}{4} = \left(\dfrac{\partial\omega}{\partial a^2}\right)\Bigg|_{\omega_0}$ $= -\dfrac{n_0\hat{\beta}_3}{2} = -\dfrac{2n_0}{\omega_0}\left(\dfrac{\partial\omega}{\partial a^2}\right)\Bigg|_{\omega_0}$. If $n_2>0$ or equivalently $\hat{\beta}_3 < 0$, and $k_2 < 0$ implying $\upsilon_g' > 0$ since $\upsilon_g' = -\upsilon_g^3 k_2$, we have a solitary wave or one-soliton solution of the form:

$$u_e = 2\mathrm{K}'\sqrt{-\frac{\upsilon_g'}{\omega_0\hat{\beta}_3}}\,\mathrm{sec}\,h\left(\mathrm{K}'Z'\right)e^{-j\frac{\upsilon_g'\mathrm{K}'^2T'}{2}}. \tag{2}$$

Let $\gamma' = -\dfrac{\omega_0\hat{\beta}_3}{4}$, $z = \dfrac{T'}{T_0}$, $\tau = \dfrac{Z'}{L_D}$, $\tilde{u}_e = \left(\dfrac{\gamma' L_D^2 u_e^2}{|\upsilon_g'|}\right)^{\frac{1}{2}}$, $L_D^2 = |\upsilon_g'|T_0$. Upon replacing these quantities in Eq. (1), we get:

$$j\frac{\partial\tilde{u}_e}{\partial z} - \frac{1}{2}\frac{\partial^2\tilde{u}_e}{\partial^2\tau} - |\tilde{u}_e|^2\tilde{u}_e = 0, \tag{3}$$

which is the normalized form of the NLS equation, and correspondingly has a single soliton solution of the form [14]:

$$\tilde{u}_e = \mathrm{K}\, sec\, h(\mathrm{K}\tau) e^{-j\frac{\mathrm{K}^2 z}{2}}. \tag{4}$$

Figure 1(a) shows the first order soliton described by Eq. (4) as it propagates in a nonlinear dispersive medium. Figure 1(b) shows the evolution of the corresponding second order soliton which can be found numerically by starting with an initial profile which is twice the amplitude of the first order soliton [14].

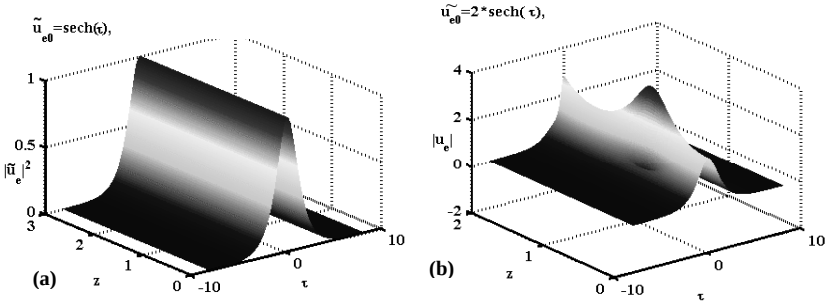

Figure 1. (a) First and (b) second order 1-D soliton evolution.

2.2 Beam propagation in bulk media: Self-focusing equation

Self-focusing is a nonlinear phenomenon, which has been studied extensively for the last four decades. Similar to the one dimensional case, the refractive index is affected by the nonlinearity. Self-focusing results in increase in the on-axis intensity and the narrowing of the beam width. For powers above a certain critical power P_c [15,16], the beam theoretically collapses with an intensity so high that it can either cause breakdown in the material, triggering some other physical effects, such as saturation of the index of refraction or failure of the assumptions about slowly varying amplitude and paraxial approximation, causing periodic focusing and defocusing. Zakharov and Shabat [17] pointed out that if the nonlinearity is strong enough this results in higher index of refraction towards the center of the beam and on-axis rays undergo total internal reflection and are thereby trapped. Nonlinearity can balance diffraction of a beam in one dimension, resulting to the formation of first order spatial solitons. Also, if the nonlinear effect is higher than diffraction, periodic focusing occurs, or may result in higher order solitons. This may not be the case in two or three dimensions where spatial collapse may occur.

The self-focusing equation in 1 and 2 transverse dimensions can be derived as in Ref. [13] where we get the following relation:

$$2jk_0 \frac{du_e}{dZ'} = \nabla_T^2 u_e - \frac{\hat{\beta}_3 k_0^2}{2} u_e^2 u_e^* \cdot \tag{5}$$

If u_e(X', Y',Z') = *a (X',Y')*$e^{-j\kappa Z'}$ is assumed to be the solution of the above equation then we have:

$$\nabla_T^2 a = 2\kappa k_0 a + \hat{\beta}_3 \frac{k_0^2}{2} a^3 \cdot \tag{6}$$

A. One-transverse dimension

Eq. (6) becomes:

$$\frac{d^2 a}{dX'^2} = +2\kappa k_0 a + \hat{\beta}_3 \frac{k_0^2}{2} a^3, \tag{7}$$

implying $X' = \int \frac{da}{\left[2\kappa k_o a^2 + \left(\hat{\beta}_3 \frac{k_0^2}{4}\right) a^4\right]^{\frac{1}{2}}}$, which is an elliptic integral, having a spatial soliton solution of the form: *a(X') = Asec h*(K*X')*, where $A = \left(-\frac{8\kappa}{\hat{\beta}_3 k_0}\right)^{\frac{1}{2}}$, *and* $K = (2\kappa k_0)^{\frac{1}{2}}$. *A,* and K are positive for $\hat{\beta}_3 < 0$ *or* $n_2 > 0$ & $\kappa > 0$. The soliton forms as a balance between focusing due to nonlinearity or self refraction, and spreading due to diffraction.

B. Two-transverse dimensions

If we consider problems of cylindrical symmetry where $\nabla_T^2 = \frac{\partial}{\partial X'^2} + \frac{\partial}{\partial Y'^2}$ $= \frac{d^2}{dr'^2} + \frac{1}{r'}\frac{d}{dr'}$, and make the transformations: $a = \left(-\frac{2\kappa}{\hat{\beta}_3 k_0}\right)^{\frac{1}{2}} \tilde{a}$, $r' = \frac{1}{(2\kappa k_0)^{\frac{1}{2}}} \tilde{r}$,

Eq. (6) becomes:

$$\frac{d^2 \tilde{a}}{d\tilde{r}^2} + \frac{1}{\tilde{r}}\frac{d\tilde{a}}{d\tilde{r}} - \tilde{a} + \tilde{a}^3 = 0, \tag{8}$$

which has no analytic solution, and is very sensitive to initial conditions. Particular solutions or modes of Eq. (8) with $\tilde{a}'(0) = 0$, $\tilde{a}(\infty) = 0$ are called the

Townes "solitons". These modes depend on the initial condition $\tilde{a}(0) = a_0$. The first three "modes" are shown in Figure 2.

C. Three dimensions

To find a stationary particular solution in this case, it is sometimes easier to start with the nonlinear Klein-Gordon (NKG) equation which may also be used to describe the envelope propagation in the presence of a cubic nonlinearity [1]. Here, the linear part of the equation can be derived from the dispersion relation: $\omega^2 = c^2{}_0 k^2 - A_1$, by replacing ω, k by the equivalent operators [1], and heuristically introducing a cubic nonlinear term (similar to the NLS):

$$\frac{\partial^2 u}{\partial T^2} - \upsilon_{p0}^2 \nabla^2 u = A_1 u + A_3 u^3, \tag{9}$$

where $A_1 > 0$, $A_3 < 0$. The relationships between A_1, A_3 and the commonly used dispersion and nonlinearity parameters can be found in Refs. [1,13]. If we consider radial symmetry, stationary solutions may be obtained by substituting $u \to u(X, Y, Z - \upsilon T)$, $(Z - \upsilon T) = \left(1 - \upsilon^2 / \upsilon_{p0}^2\right)^{1/2} Z'$, $X' = X$, $Y' = Y$. Upon neglecting all angular dependences, we get:

$$\nabla^2 u = \frac{\partial^2 u}{\partial r'^2} + \frac{D-1}{r'} \frac{\partial u}{\partial r'} = \frac{\left(A_1 u + A_3 u^3\right)}{\upsilon_{p0}^2}. \tag{10}$$

If $(D\text{-}1) = 1$, the problem is one similar to the previous case with cylindrical symmetry. If $(D\text{-}1) = 2$, the equation models the spherically symmetric case,

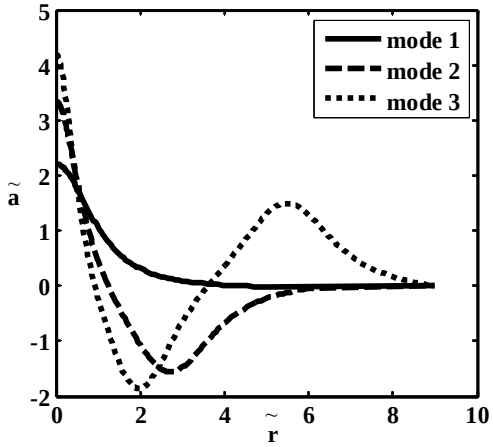

Figure 2. Townes soliton profiles.

which can give 3-D spatio-temporal solitons or optical bullets. Also, if we make a final substitution $u = \left(-\frac{A_1}{A_3}\right)^{\frac{1}{2}} \hat{a},\ \tilde{r} = A_1^{\frac{1}{2}} \frac{r'}{\upsilon_{p0}}$ in Eq. (10) we get:

$$\frac{\partial^2 \hat{a}}{\partial \tilde{r}^2} + \frac{D-1}{\tilde{r}} \frac{\partial \hat{a}}{\partial \tilde{r}} - \hat{a} + \hat{a}^3 = 0 \cdot \tag{11}$$

Figure 3 shows the 3D spatio-temporal plots or "optical bullet" propagation in bulk media where the solution tends to self-focus after propagation for some time. Figure 4 shows particular solitary wave solutions by plotting $\frac{\hat{a}(\tilde{r})}{\hat{a}(0)}$ versus $\tilde{r}$ (dotted curve) and compares it to with corresponding solutions for D =(*1,2*) (solid and dashed curves, respectively) [18].

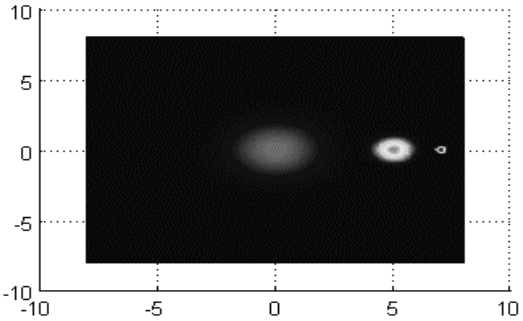

Figure 3. Optical bullet propagation. Simulation performed using numerical techniques described below.

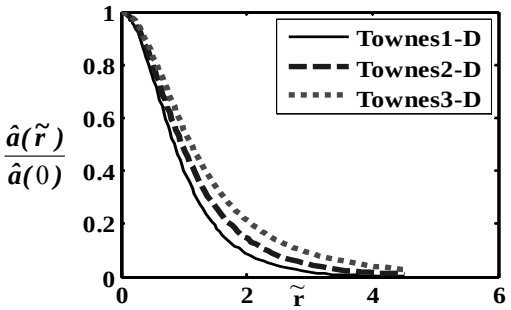

Figure 4. Townes soliton profiles for D=1 (solid line), 2 (dashed line), 3 (dotted line) (Nehmetallah and Banerjee [33]).

2.3 Nonparaxial assumption in the NLS equation

During the last stages of self-focusing, the assumptions about slowly varying amplitude and the paraxial approximation may not be valid for large focusing angles. It has been proposed that there is no singularity if one accounts for nonparaxiality [19]. Starting from Eq. (5) the paraxial and nonparaxial NLS equation which is classically used to model the self-focusing phenomenon can be written in the general operator form:

$$\frac{\partial \widetilde{u}_e}{\partial z} - j\varepsilon \frac{\partial^2 \widetilde{u}_e}{\partial z^2} = jL_r \widetilde{u}_e + jN_{nl}\left(\widetilde{u}_e\right)\widetilde{u}_e,\ \vec{r} \in \Re^D,\ z \geq 0;\ \widetilde{u}_e\left(r, z=0\right) = \widetilde{u}_{e0}\left(r\right), \qquad (12)$$

where D is the transverse dimension in space, $\varepsilon = (\lambda/4\pi r_0)^2$ and r_0 is the initial beam radius, and where $L_r \widetilde{u}_e = \Delta_T \widetilde{u}_e$, $N_{nl}\left(\widetilde{u}_e\right) = \left|\widetilde{u}_e\right|^{2\breve{\sigma}}$. For notational convenience, the z in (12) is the normalized form of Z' in Eq. (5).

2.4 Beam propagation in saturating nonlinearity

As we mentioned earlier, self-focusing results in the narrowing of the spatiotemporal pulse width in dimensions and increase in the on-axis intensity. For powers above a certain threshold the spatiotemporal pulse undergoes collapse. In reality, the high pulse intensity may either cause breakdown in the material, or some other physical effects may be triggered, such as saturating of the index of refraction, so that no further focusing may occur. The time-dependent (3+1)-dimensional (D=3) paraxial wave equation, in the presence of group velocity dispersion is [4,18,20]:

$$j\frac{\partial u_e}{\partial Z'} + \frac{1}{2k_0}\left(\frac{\partial^2 u_e}{\partial X'^2} + \frac{\partial^2 u_e}{\partial Y'^2}\right) - \frac{k_2}{2}\frac{\partial^2 u_e}{\partial T'^2} + \Gamma\left(\left|u_e\right|^{2\breve{\sigma}}\right)u_e = 0, \qquad (13)$$

where $\Gamma\left(\left|u_e\right|^{2\breve{\sigma}}\right) = \dfrac{k_0}{n_0}\delta n\left(\left|u_e\right|^{2\breve{\sigma}}\right)$ is the (saturating) nonlinear parameter responsible for self-phase modulation (SPM). For $\breve{\sigma} = 1$, $\delta n\left(\left|u_e\right|^2\right) = n_2\left|u_e\right|^2 + n_4\left|u_e\right|^4$ is the intensity induced change in index where $n_4 \neq 0$ and negative in the case of saturable nonlinearity.

Introducing the following normalization for Eq. (13): $z = \dfrac{Z'}{L_d}$, $x = \dfrac{X'}{w_0}$, $y = \dfrac{Y'}{w_0}$, $\tau = \dfrac{T'}{\left(w_0^2 k_0 k_2\right)^{1/2}}$, $\widetilde{\gamma}\left(\left|\widetilde{u}_e\right|^{2m}\right) = L_d\Gamma\left(\left|u_e\right|^{2\breve{\sigma}}\right)$, $L_d = 2k_0 w_0^2$, we arrive at

$$j\frac{\partial \widetilde{u}_e}{\partial z} + \left(\frac{\partial^2 \widetilde{u}_e}{\partial x^2} + \frac{\partial^2 \widetilde{u}_e}{\partial y^2} - s_d\frac{\partial^2 \widetilde{u}_e}{\partial \tau^2}\right) + \widetilde{\gamma}\left(\left|\widetilde{u}_e\right|^{2\breve{\sigma}}\right)\widetilde{u}_e = 0, \qquad (14)$$

where $s_d = sgn(k_2)$ ($sgn(x) = -1,1$ for $x<0$, $x>0$ respectively), w_0 is the initial transverse spatial width, and L_d is the diffraction length. If $s_d = -1$ (anomalous dispersion) we can assume spherical symmetry of the field distribution and introduce the radial variable $r = (x^2 + y^2 + \tau^2)^{1/2}$ to recast Eq. (14) as [20]

$$j\frac{\partial \tilde{u}_e}{\partial z} + \frac{1}{r^{D-1}}\frac{\partial}{\partial r}\left(r^{D-1}\frac{\partial \tilde{u}_e}{\partial r}\right) + \tilde{\gamma}\left(\left|\tilde{u}_e\right|^2\right)\tilde{u}_e = 0\,, \tag{15}$$

where D is *3* and $\ddot{\sigma} = 1$ and $\tilde{\gamma}(\tilde{u}_e) = \dfrac{\tilde{u}_e}{1+\mu\tilde{u}_e} \approx \tilde{u}_e - \mu\tilde{u}_e^{\,2}$ in our case.

2.5 Dispersion management in D-dimensions

In the last decade, dispersion management (DM) techniques have received a lot of attention due to their advantages in high speed nonlinear wave propagation in optical communication systems. One of these advantages is the enormous reduction of the inter-pulse effects due to the zero dispersion limit [21]. In 1 dimension (1D) DM reduces pulse radiation due to modulation instability reduction, it also reduces amplitude compensating fiber loss and jitter due to collisions between signals in different channels of wavelength division multiplexed systems (WDMS). Also, DM has many other effects which provides stabilizing pulse propagation for very long distances [22]. Hence, DM is expected to be the future of soliton-based communication systems. The time-dependent paraxial wave equation, in the presence of periodic modulation of dispersion, has the form of a modified (D+1)-dimensional NLS with a dimensionless envelope of the optical field according to

$$j\frac{\partial \tilde{u}_e}{\partial z} + \frac{f(z)}{2}\frac{1}{r^{D-1}}\frac{\partial}{\partial r}\left(r^{D-1}\frac{\partial \tilde{u}_e}{\partial r}\right) + \left|\tilde{u}_e\right|^2\tilde{u}_e = 0\,, \tag{16}$$

where $r = (x^2 + y^2)^{1/2}$ or $r = (x^2 + y^2 + \tau^2)^{1/2}$ for cylindrical ($D=2$) or spherical ($D=3$) symmetry of the field distribution respectively, and f (z) is either piecewise continuous (PWC) periodic functions or simple harmonic functions of the form $\vartheta(z) = \vartheta_0 + \vartheta_1 \sin \Omega z$.

2.6 Nonlinearity management in D-dimensions

Some studies show that beam stabilization can be accomplished if the nonlinearity coefficient is weakly modulated along the propagation direction where the beam power oscillates about the modulated critical value [23]. Also, Towers and Malomed [24] concluded that a better stabilization can be obtained if we use a more radical modulation of the nonlinearity. This modulation is done based on a periodically alternating self-focusing (SF) and self defocusing

(SDF) layers or even a stack of periodic SF layers with different values of the Kerr coefficient. Note that in a quadratically nonlinear medium with phase mismatch ΔK, it has been shown that the effective cubic nonlinearity coefficient, $\chi_{eff}^{(3)}(z) \propto \left(\chi^{(2)}\right)^2 \left(\frac{1-\exp(-j\Delta K z)}{\Delta K}\right)$, will be automatically periodic [25].

The time-dependent ($D+1$)-dimensional ($D=3$) paraxial wave equation in the presence of group velocity dispersion is [4, 18]:

$$j\frac{\partial u_e}{\partial Z'} + \frac{1}{2k_0}\left(\nabla_\perp^2 u_e\right) - \frac{k_2}{2}\frac{\partial^2 u_e}{\partial T'^2} + \hat{g}(Z')\left|u_e\right|^2 u_e = 0, \tag{17}$$

where $\hat{g}(Z') = n_2(Z')\,k_0/n_0$ is the nonlinear parameter responsible for SPM and is either piecewise continuous in layers of width L or harmonic function of period L. Introducing the following normalization for Eq. (17): $z = \frac{Z'}{L_d}$, $x = \frac{X'}{w_0}$, $y = \frac{Y'}{w_0}$, $\tau = \frac{T'}{\left(w_0^2 k_0 k_2\right)^{1/2}}$, $\tilde{u}_e = \left(L_d\right)^{1/2} u_e$, $L_d = k_0 w_0^2$, we arrive at

$$j\frac{\partial \tilde{u}_e}{\partial z} + \frac{1}{2}\left(\nabla_\perp^2 \tilde{u}_e - s_d\frac{\partial^2 \tilde{u}_e}{\partial \tau^2}\right) + g(z)\left|\tilde{u}_e\right|^2 \tilde{u}_e = 0, \tag{18}$$

where $s_d = sgn(k_2)$, w_0 is the initial transverse spatial width, L_d is the diffraction length and where $\hat{g}(Z') = g(z)$. If we assume s_d = -1 (anomalous dispersion) and spherical symmetry of the field distribution, and introduce the radial variable $r = (x^2 + y^2 + \tau^2)^{1/2}$, Eq. (18) can be written as

$$j\frac{\partial \tilde{u}_e}{\partial z} + \frac{1}{2}\frac{1}{r^{D-1}}\frac{\partial}{\partial r}\left(r^{D-1}\frac{\partial \tilde{u}_e}{\partial r}\right) + g(z)\left|\tilde{u}_e\right|^2 \tilde{u}_e = 0, \tag{19}$$

where D can take on any value from 1 to 3.

3. Hankel or Fourier Bessel transform methods

Most of the PDEs mentioned so far do not have a closed form solution, and hence we use numerical techniques to tackle these types of problems. However, due to the computational complexity of the problem encountered in higher dimensions, we have shifted our focus towards numerical integral transform techniques and their variations to solve such type of equations. In this Section we outline a numerical technique called the adaptive fast Hankel split step (AFHSS) [26-31] or adaptive Fourier Bessel split step (AFBSS) method. This method is used to track, as an example, the solutions of the 2 and 3-D NLS equation and their variations. Note that this method is based on

the combination of the standard split step fast Fourier transform (SSFFT) technique and the use of the Hankel transform, which utilizes the cylindrical and spherical symmetry of the problem. This symmetry leads us to use this method applied to the above problem. Also, we remark that the computation time and precision are enhanced enormously. In addition to this tool, we will also use the similarity criterion developed by Zakharov *et al.* [17]. This criterion is applied to transverse spatial dimensions and the longitudinal propagation step, which can be adaptively updated. In this way, we can track the pulse/beam amplitudes to distances very close to the collapse distance in the self-focusing case and can also track the amplitude dynamics of the spatiotemporal solitons, as discussed later.

The AFHSS algorithm in Figure 5 resembles the symmetrized Fourier split-step technique, but where we change the longitudinal propagation stepping size $\Delta z \propto A\,(z_1)^{-1/s} - A(z_2)^{-1/s} \approx A(z_1)^{-1/s}$ when $A(z_2) >> A(z_1)$ adaptively using the similarity formula defined in [17] where $s = (2/3,1/2)$ for $D = (2,3)$ respectively, and the grid spatial range $\Delta r_{\max} \propto A(z)^{1-D}$ in order to track the varying amplitude of the spatio-temporal pulse in the medium. The flowchart in Figure 5 has been written for the time-dependent paraxial wave equation, in the presence of periodic modulation of dispersion and nonlinearity, which, as discussed above, has the form of a modified (D+1)-dimensional NLS for a dimensionless envelope of the optical field:

$$j\frac{\partial \tilde{u}_e}{\partial z} + \frac{1}{2}\frac{f(z)}{r^{D-1}}\frac{\partial}{\partial r}\left(r^{D-1}\frac{\partial \tilde{u}_e}{\partial r}\right) + g(z)\left|\tilde{u}_e\right|^2\tilde{u}_e = 0 \cdot \tag{20}$$

The linear operator in Eq. (20) with *D=2,3* is

$$\left(\frac{\partial^2}{\partial r^2} + \frac{D-1}{r}\frac{\partial}{\partial r}\right)\tilde{u}_e \cdot \tag{21}$$

The Hankel transform or Fourier Bessel technique can not apply directly to this operator in the case when *D=3*, so we have to transform the operator from spherical coordinates to cylindrical coordinates by letting $\tilde{u}_e(r,z) = r^{-l}v(r,z)$, where *l* is the order of the Fourier Bessel or Hankel transform. The expression (21) then becomes $\left(\frac{\partial^2}{\partial r^2} + \frac{1}{r}\frac{\partial}{\partial r} - \frac{l^2}{r^2}\right)v \xrightarrow{AFHSS} -4\pi^2\rho^2 v_{\mathcal{H}}(\rho,z)$, where $v_{\mathcal{H}}(\rho,z) = \mathcal{H}_l\left[v(r,z)\right] = \mathcal{H}_l\left[r^l\tilde{u}_e(r,z)\right] \Rightarrow \tilde{u}_e(r,z) = r^{-l}\mathcal{H}_l\left[v_{\mathcal{H}}(\rho,z)\right]$, with $l = 0, \frac{1}{2}$ in the case of the cylindrical and spherical Fourier Bessel transform pair respectively, where they are related to each other by:

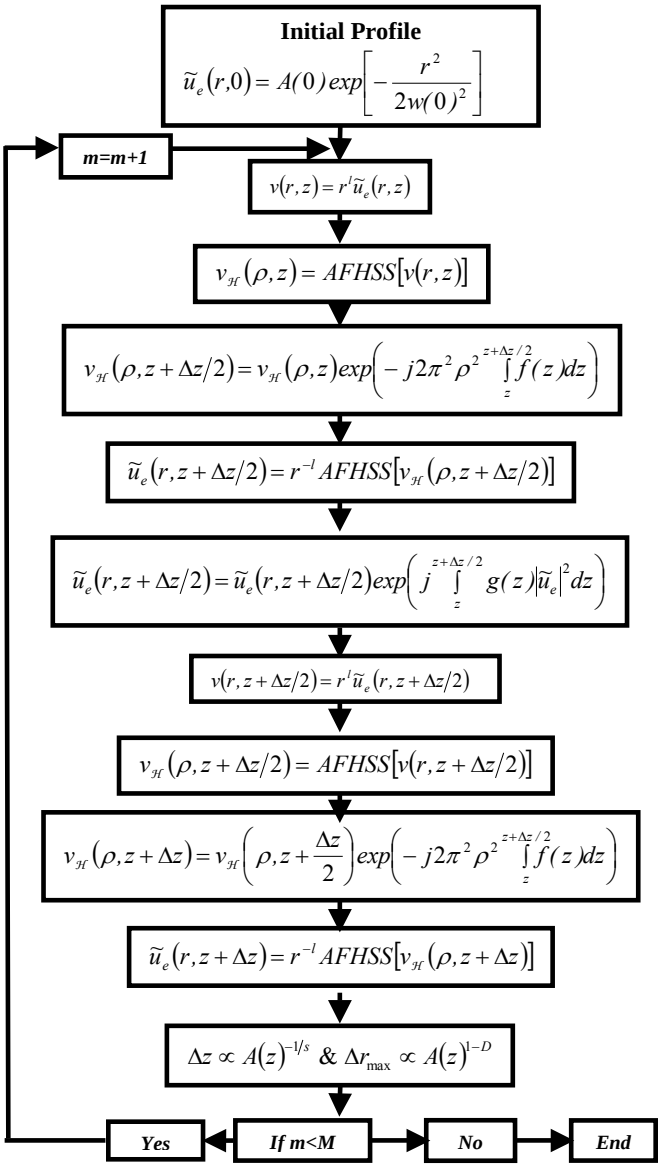

Figure 5. The AFHSS algorithm, a symmetrized version of the split step FFT using cylindrical or spherical Fourier Bessel transform instead, and using adaptive longitudinal stepping and transverse grid management (Nehmetallah and Banerjee [37]).

$$\tilde{u}_e(r,z)=\int_0^{\infty}\tilde{u}_{e\mathcal{H}}(\rho,z)j_{l-1/2}(\rho r)\rho^{l+3/2}d\rho=\sqrt{\frac{\pi}{2}}r^{-l}\int_0^{\infty}\rho^{l+1}\tilde{u}_{e\mathcal{H}}(\rho,z)J_l(\rho r)d\rho, \tag{22}$$

$$\tilde{u}_{e\mathcal{H}}(\rho,z)=\frac{2}{\pi}\int_0^{\infty}\tilde{u}_e(r,z)j_{l-1/2}(\rho r)r^{l+3/2}dr=\sqrt{\frac{2}{\pi}}\rho^{-l}\int_0^{\infty}r^{l+1}\tilde{u}_e(r,z)J_l(\rho r)dr, \tag{23}$$

where $j_l(x)=(-x)^l\left(\frac{1}{x}\frac{d}{dx}\right)^l\frac{sin(x)}{x}=\sqrt{\frac{\pi}{2x}}J_{l+1/2}(x)$ is the l^{th} order spherical Bessel function. The above transform pair is solved by the l^{th} order finite Hankel Transform method, explained in the next subsection.

3.1 Calculation of the Hankel transform

Many techniques are used to calculate the Hankel transform [26, 27] but we adopted Yu's [28] or Guizar's [29] method. We use the definition of the l^{th} order finite Hankel Transform of the third kind [30]:

$$\mathcal{H}[\tilde{u}_e(r,z)]=\tilde{u}_{e\mathcal{H}}(\rho_m,z)=\int_q^p r\tilde{u}_e(r,z)[J_l(r\rho_m)Y_l(q\rho_m)-J_l(q\rho_m)Y_l(r\rho_m)]dr, \tag{24}$$

in which ρ_m's are the roots of the transcendental equation $J_l(q\rho_m)Y_l(P\rho_m) - J_l(q\rho_m)Y_l(q\rho_m) = 0$, the inverse transform can be written as

$$\tilde{u}_e(r,z)=\frac{\pi^2}{2}\sum_m\frac{\rho_m^2J_l^2(\rho_m p)u_{\mathcal{H}}(\rho_m,z)}{J_l^2(\rho_m q)-J_l^2(\rho_m p)}\times[J_l(\rho_m r)Y_l(q\rho_m)-J_l(\rho_m q)Y_l(r\rho_m)]. \tag{25}$$

For $q=0$ and $\rho_m=\frac{\kappa_{lm}}{2\pi p}$ Eq. (25) becomes [30] $\tilde{u}_e(r,z)=\sum_m\breve{c}_{lm}J_l\left(\kappa_{lm}\frac{r}{p}\right), 0\le r\le p,$

where $\breve{c}_{lm}=\frac{1}{p^2J_{l+1}^2(\kappa_{lm})}\int_0^a r\tilde{u}_e(r,z)J_l\left(\kappa_{lm}\frac{r}{p}\right)dr$ and $J_l(\kappa_m)=0$. Let us evaluate the radius r at $r_n=\frac{\kappa_{ln}}{2\pi R_2}$ and the frequency at $\rho_m=\frac{\kappa_{lm}}{2\pi R_1}$, $r_n\in r \ge \mathrm{R}_1 = p$ & $\rho_m\in\rho\ge R_2$, we have $\tilde{u}_e(r_n)=\tilde{u}_{e\mathcal{H}}(\rho_m)=0$, where R_1, R_2 are the spatial and transform ranges respectively, with $\tilde{S}=2R_1R_2$. From above, we can write the expansion of the function and its transform by an l^{th} order Bessel series [28, 29]

$$U_{\mathcal{H}}(m)=\sum_{n=1}^{N}C_{mn}U(n),\ U(n)=\sum_{m=1}^{N}C_{nm}U_{\mathcal{H}}(m), \tag{26a}$$

$$C_{mn}=\frac{2}{\tilde{S}}J_l\left(\frac{\kappa_{ln}\kappa_{lm}}{\tilde{S}}\right)\left|J_1^{-1}(\kappa_{ln})\right|\left|J_1^{-1}(\kappa_{lm})\right|, \tag{26b}$$

$$U(n) = \tilde{u}_e\left(\frac{\kappa_{ln}}{2\pi R_2}, z\right)\left|J_{l+1}^{-1}(\kappa_{ln})\right|R_1,$$

$$U_{\mathcal{H}}(m) = \tilde{u}_{e\mathcal{H}}\left(\frac{\kappa_{lm}}{2\pi R_1}, z\right)\left|J_{l+1}^{-1}(\kappa_{lm})\right|R_2. \qquad (26c)$$

Here it is preferable to choose R_2 as large as possible, and R_1 is determined by the initial profile, which is going to decrease due to focusing in this problem. Also, if we choose $\tilde{S} = \kappa_{lN+1}$, then the error is close to zero as N increases.

4. Focusing arrest mechanisms

As explained earlier, self-focusing results in the narrowing of the beam width in two transverse dimensions and increases the on-axis intensity. Above a certain threshold power the beam undergoes collapse. Although the exact value of the critical power depends on the spatial distribution of the input beam, the critical power of circularly symmetric beams is not more than a few percent above the theoretical lower bound value [15, 16] $P_c^{lb} = \frac{\lambda^2}{4\pi n_0 n_2}\mathcal{N}_c$, where $\mathcal{N}_c$ is the normalized beam power, which is a necessary condition for collapse. The slowly varying amplitude and the paraxial approximation assumptions are not valid for large focusing angles during the last stages of self-focusing, and there is no singularity if one accounts for nonparaxiality [19].

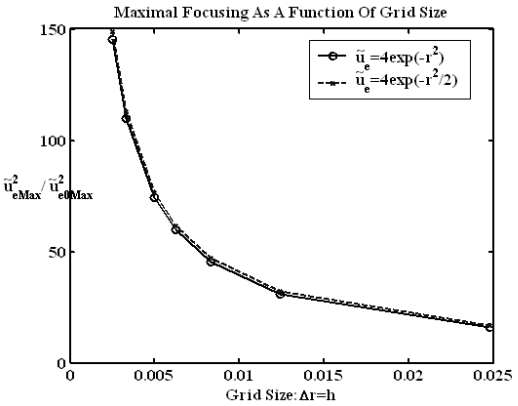

Figure 6. Maximal focusing as a function of grid size (Banerjee et al. [31]).

For a problem with cylindrical symmetry, the Hankel transform technique is preferable over other classical techniques such as finite difference, finite element, and wavelet methods, due to the availability of fast algorithms with speeds comparable to one-dimensional fast Fourier transform (FFT) methods. For a detailed study of the nonparaxial NLS, refer to Ref. [31]. Numerically we used the AFHSS algorithm developed earlier to solve Eq. (12).

Figure 6 shows the maximal focusing as a function of grid size $h = \Delta r$ which proves the convergence of our methods to the numerical focusing point when Δr decreases by varying the $\widetilde{S}$ parameter defined above. Although the trend is similar, this is a considerable improvement over the convergence test results in Fibich and Ilan [32]. Figure 7 shows the growth of the on-axis intensity using the AFHSS technique for a Gaussian test function.

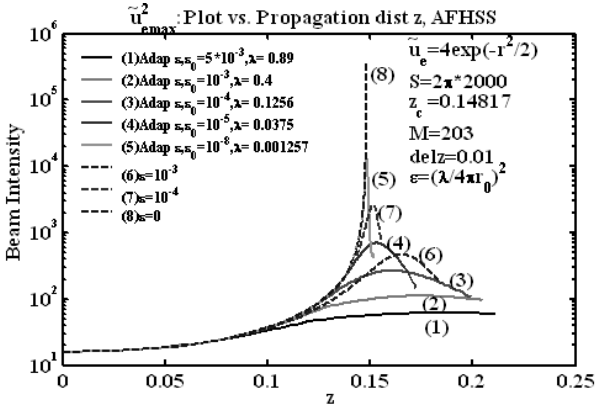

Figure 7. On-axis intensity of $\tilde{u}_{e0} = 4exp(-r^2/2)$ as a function of propagation for fixed values of ε ranging from 10^{-2} to 10^{-8} where $z = z_c = 0.1481$ for $\varepsilon = 10^{-8}$, and for an adaptive ε varying as $\varepsilon = (\lambda/4\pi r)^2$, using AFHSS with $\widetilde{S} = 2\pi R_1 R_2 = 2\pi \times 2000$ (4000 cylindrical samples). λ in inset is normalized to r_0. (Banerjee *et al*. [31]).

5. Saturating nonlinearity

When a pulsed optical beam propagates through a bulk nonlinear medium, it is affected by diffraction, (anomalous) dispersion, and nonlinear refraction. Such a space-time combined effect lead to many nonlinear phenomena such as spatiotemporal collapse, which can yield short pulses with extremely high optical fields, or formation of three dimensional optical solitons or light bullets [18]. These light bullets represent an extension of self-trapped optical beams into the temporal domain. Such optical solitons are important in tele-

communication systems due to their self-confined structure, by preserving their shape after propagating long distances, where they satisfy the requirement of being self-guided in bulk media. Under the combined and balanced effect of linear diffraction and dispersion and the spatio-temporal nonlinear effect, optical bullets may exist. The above phenomenon is traditionally governed by the (3+1)-dimensional NLS, which can be viewed as a limit of the Zakharov system of Langmuir waves in plasma. Note that in (1+1)-dimensions, the NLS equation can be solved explicitly by the inverse scattering method [3] and particular solutions are stable, corresponding to temporal or spatial solitons. However, in (2+1) and (3+1)-dimensional cases, solutions are not stable and they can be stabilized by using saturating nonlinearities or graded-index nonlinear media for example [19, 33].

In this Section we use the AFBSS method, to numerically solve Eq. (15) with and without saturating nonlinearity, which is classically used to model this phenomenon. For a detailed study refer to Ref. [33]. Figure 8 shows that a beam will start to focus, and then self-trapping occurs during to saturation nonlinearity for the following pulse parameters $N_0 = 50, A_0^2 = 0.4, w_0 = 5$, where N_0, A, w, are the normalized power, amplitude and width respectively.

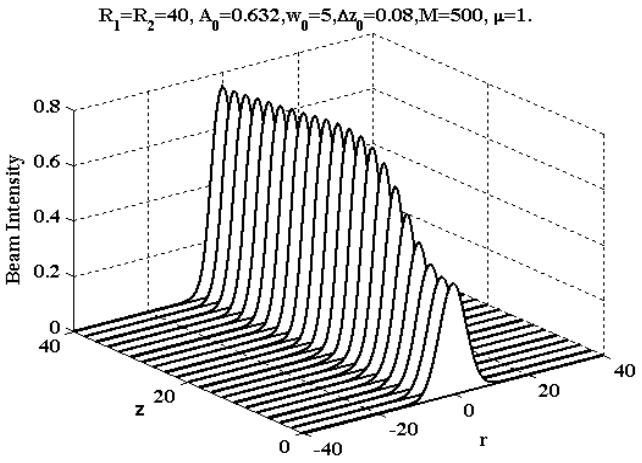

Figure 8. Stable light-bullet generation with initial focusing (Nehmetallah and Banerjee [33]).

6. Dispersion management

As mentioned in Section 2.5, DM has received a lot of attention due to its benefits in high-speed optical communications systems. Analytical study is

necessary to understand fundamental pulse dynamics and the interaction between dispersion fluctuation and nonlinearity. Several different methods have been developed to study pulse propagation in DM fibers each has its region of applicability to successfully describe the pulse dynamics of the DM solitons. In 1-D, a novel technique based on wavelet transform to numerically solve pulse propagation in a nonlinear optical fiber with periodically modulated dispersion is used. Readers are referred to Ref [34] for details on the adaptive wavelet transform (AWT) method. Moreover, an analytical description for the chirped pulse dynamics based on the Lagrangian theory is also presented, in which the average dispersion is in the anomalous regime and where we obtain good agreement between this analytical method and AWT.

6.1 Variational technique

In this Section we reduce Eq. (20) with a periodic dispersion (and nonlinearity) map using a variational technique to a coupled set of nonlinear ordinary differential equations (ODEs). These ODEs accurately predict the pulse dynamics in (a) both a weak and strong nonlinear medium, compared to dispersion, and (b) slow or fast modulation frequency, compared to the frequency of oscillations of the soliton width. This analytical method defines the boundaries for how to select stable initial conditions for the pulse and the dispersion map, and we use this information in our numerical technique to solve (20).

In the presence of periodic modulation of dispersion and nonlinearity, the functions $f(z)$, $g(z)$ in the equation

$$j\frac{\partial \tilde{u}_e}{\partial z}+\frac{f(z)}{2}\frac{1}{r^{D-1}}\frac{\partial}{\partial r}\left(r^{D-1}\frac{\partial \tilde{u}_e}{\partial r}\right)+g(z)\left|\tilde{u}_e\right|^2\tilde{u}_e=0 \tag{27}$$

are either piecewise continuous (PWC) periodic functions or simple harmonic functions of the form $\mathcal{G}(z)=\mathcal{G}_0+\mathcal{G}_1 \sin\Omega z$.

The variational approach describes the wave evolution based on the Lagrangian formalism of classical mechanics in terms of the Lagrangian density [35]

$$\mathcal{L}=\frac{j}{2}\left(\tilde{u}_e^{\,*}\frac{\partial \tilde{u}_e}{\partial z}-\tilde{u}_e\frac{\partial \tilde{u}_e^{\,*}}{\partial z}\right)r^{D-1}+\frac{f(z)}{2}\left|\frac{\partial \tilde{u}_e}{\partial r}\right|^2 r^{D-1}-\frac{1}{2}r^{D-1}g(z)\left|\tilde{u}_e\right|^4, \tag{28}$$

where the (D+1) NLS equation can be derived from $\mathcal{L}$ using the Euler-Lagrange equation

$$\frac{\partial}{\partial z}\frac{\partial \mathcal{L}}{\partial\left(\partial \widetilde{u}_e / \partial z\right)}+\frac{\partial}{\partial r}\frac{\partial \mathcal{L}}{\partial\left(\partial \widetilde{u}_e / \partial r\right)}-\frac{\partial \mathcal{L}}{\partial \widetilde{u}_e}=0 \cdot \tag{29}$$

Note that the application of Eq. (29) to the Lagrangian density in Eq. (28) generates the NLS equation given in Eq. (27). Following the Ritz optimization procedure, let us assume the initial profile to be one of the following forms:

$$\widetilde{u}_e=\widetilde{u}_e(r,z)=A(z)exp\left[-\frac{r^2}{2w^2(z)}+jb(z)r^2\right],$$

$$\widetilde{u}_e(r,z)=A(z)sec\,h\left(\frac{r}{w(z)}\right)exp\left[jb(z)r^2\right], \tag{30}$$

where the amplitude *A(z)*, beam radius *w(z)*, and wave-front curvature *b(z)*, are unknown functions of the propagation distance *z*. Following the method in [35], where we insert the trial functions from Eq. (30) into the Lagrangian and by integrating:

$$\begin{aligned}\langle \mathcal{L} \rangle &= \int_0^\infty \mathcal{L}dr=\frac{i}{2}\left(A\frac{dA^*}{dz}-A^*\frac{dA}{dz}\right)w^D\alpha_{D-1}+|A|^2 w^{D+2}\left(\frac{db}{dz}+2fb^2\right)\alpha_{D+1}\\ &+\frac{f}{2}|A|^2 w^{D-2}\gamma_{D-1}-\frac{1}{2}w^D\beta_{D-1}g(z)|A|^4,\end{aligned} \tag{31}$$

we obtain the reduced Lagrangian, where the α, β, and γ's are given by

$$\alpha_D=\int_0^\infty r^D\exp\left(-r^2\right)dr,\ \beta_D=\int_0^\infty r^D\exp\left(-2r^2\right)dr,\ \gamma_{D-1}=\alpha_{D+1}, \tag{32}$$

for a Gaussian ansatz, and

$$\alpha_D=\int_0^\infty r^D\sec h^2(r)dr,\ \beta_D=\int_0^\infty r^D\sec h^4(r)dr,\ \gamma_D=\alpha_D-\beta_D, \tag{33}$$

for a hyperbolic secant assumption.

We can derive a set of evolution equations called Euler-Lagrange equations taking into account that the variation with respect to the unknowns in the initial profile should be equal to zero, namely: $\frac{\delta\langle \mathcal{L} \rangle}{\delta Q}=0\Rightarrow$ $\frac{\partial\langle \mathcal{L} \rangle}{\partial Q}-\frac{d}{dz}\left(\frac{\partial\langle \mathcal{L} \rangle}{\partial Q'}\right)=0$, where $Q=\left(A,w,b,A^*\right)$. The evolution equations obtained are given by:

$$|A|^2 w^D=A_0^2 w_0^D=N_0, \tag{34a}$$

$$b = \frac{1}{2fw}\frac{dw}{dz}, \tag{34b}$$

$$\frac{d\tilde{\phi}}{dz} = \left[-\frac{\gamma_{D-1}}{\alpha_{D-1}}\frac{f(z)}{w^2} + \left(1+\frac{D}{4}\right)g(z)\frac{\beta_{D-1}}{\alpha_{D-1}}|A|^2 \right], \tag{34c}$$

$$\frac{d^2w}{dz^2} = \frac{\gamma_{D-1}}{\alpha_{D+1}}\frac{f^2(z)}{w^3} - \frac{N_0 D\beta_{D-1}}{2\alpha_{D+1}}\frac{f(z)g(z)}{w^{D+1}} + \frac{1}{f(z)}\frac{dw}{dz}\frac{df}{dz}, \tag{34d}$$

where $A(z) = |A(z)|e^{i\tilde{\phi}(z)}$, N_0 is the initial pulse energy defined above.

In what follows, we consider the case where $g(z) = 1$ for the case of dispersion management. The case $f(z) = 1$ for the case of nonlinearity management will be discussed in the following Section.

6.2 The 1-dimensional case (D=1)

If we consider the case of a harmonic and a high-frequency modulation of the dispersion map of the form $f = 1+sin\Omega z$, where $\Omega > \omega_s$ where ω_s is the soliton width oscillation frequency [21]. Also we assume the ratio f_1/Ω to be small and a hyperbolic secant ansatz as an initial pulse. Taking the derivative of Eq. (34b) and comparing it to Eq. (34d), we arrive at the following system of ODEs [21]

$$w_z = 2wbf, \tag{35a}$$

$$b_z = \frac{2f}{\pi^2 w^4} - 2b^2 f - \frac{2N_0}{\pi^2 w^3}, \tag{35b}$$

where, for notational brevity, the subscripts stand for derivatives. Following the Kapitza approach, the width w and the chirp b has the form $w = \tilde{w} + \delta w, b = \tilde{b} + \delta b$ respectively. Upon taking the average, denoted by the symbol $\langle \cdots \rangle$, of Eqs. (35a) and (35b); after gathering the slowly varying terms apart from the rapidly varying ones; assuming $\langle \tilde{w}^n \rangle = \tilde{w}^n, \langle \tilde{b}^n \rangle = \tilde{b}^n$ $\left\langle \frac{d\tilde{w}}{dz} \right\rangle = \frac{d\tilde{w}}{dz}, \left\langle \frac{d\tilde{b}}{dz} \right\rangle = \frac{d\tilde{b}}{dz}$; and dropping out the (~) for convenience, Eqs. (35a), (35b) become

$$w_z = 2wb + 2w\langle \delta w f_1 \sin\Omega z \rangle + 2b\langle \delta w f_1 \sin\Omega z \rangle + 2\langle \delta w \delta b \rangle, \tag{36a}$$

$$b_z = \frac{2}{\pi^2 w^4}\left(1+10\frac{\langle \delta w^2\rangle}{w^2}-4\frac{\langle f_1 \delta w \sin\Omega z\rangle}{w}\right)$$
$$-2b^2-2\langle \delta b^2\rangle-4b\langle \delta b f_1 \sin\Omega z\rangle-\frac{2N_0^2}{\pi^2 w^3}\left(1+\frac{6\langle \delta w^2\rangle}{w^2}\right), \tag{36b}$$

$$\delta w_z = 2wbf_1 \sin\Omega z + 2w\delta b + 2b\delta w, \tag{36c}$$

$$\delta b_z = \left(\frac{6N_0}{\pi^2 w^4}-\frac{8}{\pi^2 w^5}\right)\delta w+\left(\frac{2}{\pi^2 w^4}-2b^2\right)f_1 \sin\Omega z - 4b\delta b\cdot \tag{36d}$$

Let $\delta_b = S_1 sin\ \Omega z + S_2 cos\ \Omega z$, $\delta w = S_3 sin\ \Omega z + S_4 cos\ \Omega z$. Defining $\tilde{\kappa} = \left(\frac{6N_0}{\pi^2 w^4}-\frac{8}{\pi^2 w^5}\right)$, $\tilde{d} = \left(\frac{2}{\pi^2 w^4}-2b^2\right)f_1$, a particular solution to Eqs. (36c) and (36d) can be found from the following system of linear equations

$$\begin{bmatrix} 0 & 2w & -\Omega & 2b \\ 2w & 0 & 2b & \Omega \\ \Omega & 4b & 0 & -\tilde{\kappa} \\ 4b & -\Omega & -\tilde{\kappa} & 0 \end{bmatrix}\begin{bmatrix} S_1 \\ S_2 \\ S_3 \\ S_4 \end{bmatrix} = \begin{bmatrix} 0 \\ -2wbf_1 \\ 0 \\ \tilde{d} \end{bmatrix}. \tag{37}$$

The solution of the above system gives

$$S_1 = \frac{-2bwf_1\tilde{\kappa}\left(2w\tilde{\kappa}+8b^2+\Omega^2\right)}{\mathrm{M}}+4\frac{bd\left(w\tilde{\kappa}+\Omega^2+4b^2\right)}{\mathrm{M}}, \tag{38a}$$

$$S_2 = -4\frac{\Omega b^2 w f_1\tilde{\kappa}}{\mathrm{M}}-\frac{\Omega\tilde{d}\left(2w\tilde{\kappa}+\Omega^2+4b^2\right)}{\mathrm{M}}, \tag{38b}$$

$$S_3 = \frac{-4b^2 wf_1\left(4w\tilde{\kappa}+16b^2+\Omega^2\right)}{\mathrm{M}}-2\frac{w\tilde{d}\left(2w\tilde{\kappa}+\Omega^2+8b^2\right)}{\mathrm{M}}, \tag{38c}$$

$$S_4 = \frac{-2bwf_1\Omega\left(2w\tilde{\kappa}+\Omega^2+16b^2\right)}{\mathrm{M}}-4\frac{b\tilde{d}w\Omega}{\mathrm{M}}, \tag{38d}$$

where $\mathrm{M} = 4w^2\tilde{\kappa}^2+32wb^2\tilde{\kappa}+4w\Omega^2\tilde{\kappa}+\Omega^4+20b^2\Omega^2+64b^4$. Assuming f_1 to be sufficiently large so as to neglect the second terms in (38), we arrive at

$$\delta w = \frac{-4f_1}{\Omega^2}\left[\frac{1}{\pi^2 w^3}+1\right]sin\,\Omega z-\frac{2wbf_1}{\Omega}cos\,\Omega z, \tag{39a}$$

$$\delta b = \frac{4bf_1}{\Omega^2}\left[\frac{1}{\pi^2 w^4} + b^2\right] sin\,\Omega z - \frac{2f_1}{\pi^2\Omega} cos\,\Omega z, \tag{39b}$$

$$w_z = 2wb + \frac{f_1^2}{\Omega^2}\left(\frac{4b}{\pi^2 w^3} - 2wb^3\right), \tag{39c}$$

$$b_z = \frac{2}{\pi^2 w^4} - 2b^2 - \frac{2N_0}{\pi^2 w^3} + \frac{4f_1^2}{\pi^2\Omega^2} \times \left(\frac{12b^2}{w^4} + \frac{3}{\pi^2 w^8} - 2b^4 - 6\frac{N_0 b^2}{w^3}\right). \tag{39d}$$

The above system can be simplified if we consider f_1/Ω to be small. We obtain

$$w_{zz} = \frac{4}{\pi^2 w^3} - 4\frac{N_0}{\pi^2 w^2} + \frac{24 f_1^2}{\pi^4\Omega^2 w^7}, \tag{40}$$

which admits a fixed point solution $w = \frac{1}{N_0} + \frac{6N_0^3 f_1^2}{\pi^2\Omega^2}$, which corresponds to the potential $T = \frac{2}{\pi^2 w^2} - \frac{4N_0}{\pi^2 w} + \frac{4f_1^2}{\pi^2 w^6\Omega^2}$. Note that stabilization is possible when there is a minimum in this effective potential.

We now show sample simulation results using the AWT methods. Figure 9 shows the variation of the on-axis pulse amplitude for three different dispersion map periods, keeping the same amplitude in the anomalous dispersion regime according to condition stated above, with the initial pulse $\tilde{u}_e = 2\,exp\left(-\tau^2\right)$, using the AWT techniques according to the accompanying initial conditions.

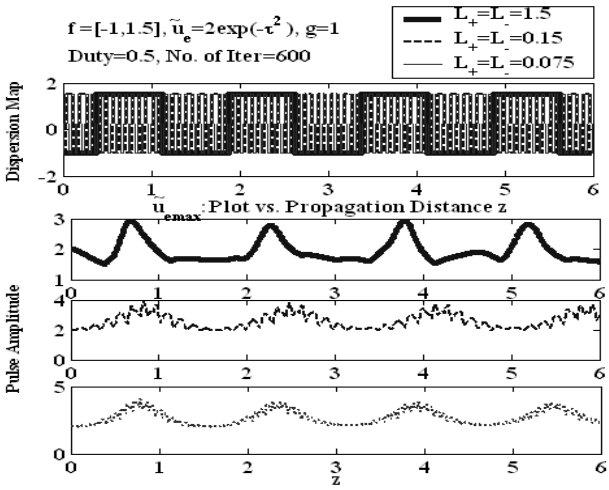

Figure 9. Variation of the on-axis pulse amplitude for three different dispersion map periods, keeping the same amplitude in the anomalous dispersion regime with the initial pulse $\tilde{u}_e = 2exp(-\tau^2)$, using the AWT techniques according to the accompanying initial conditions.

6.3 The 2-dimensional case (D=2)

In 2-D, we have to use the adaptive fast Hankel split step (AFHSS) transform developed earlier (instead of the AWT) to numerically solve the underlying nonlinear Schrödinger (NLS) equation with dispersion management terms, use the averaged variational technique to reduce the governing (D+1)-dimensional NLS equation to a coupled set of nonlinear ordinary differential equations (ODEs) and rigorously solve these equations and study their stability in each case. These ODEs accurately predict the pulse dynamics in a medium of periodic nonlinearity and/or dispersion variations. This analytical method defines the boundaries for how to select stable initial conditions for the pulse and the dispersion map, and compare it with the exact numerical technique developed.

Let us again consider a periodic function for the dispersion of the form $f(z) = f_0 + f_1 \sin\tilde{\Omega}z$. From Eqs. (34b) and (34d) we arrive at the following ODE system

$$\frac{db}{dz} = \frac{c_1 f - c_2}{2w^4} - 2fb^2, \tag{41a}$$

$$\frac{dw}{dz} = 2fbw \cdot \tag{41b}$$

Following a similar approach to the 1-dimensional case [36], we arrive at the condition $0 < f_0 < N_0\beta_1/\gamma_1$.

6.4 The 3-dimensional case (D=3)

Let us consider a periodic function for the dispersion of the form $f(z) = f_0 + f_1 \sin\tilde{\Omega}z$. Let $\varpi = wb$, then from Eqs. (34b) and (34d) we arrive at the following ODE system

$$\frac{d\varpi}{dz} = \frac{c_1 f}{w^3} - \frac{c_2}{w^4}, \tag{42a}$$

$$\frac{dw}{dz} = 2f\varpi, \tag{42b}$$

where $c_3 = \frac{\gamma_{D-1}}{2\alpha_{D+1}}, c_4 = \frac{DN_0\beta_{D-1}}{4\alpha_{D+1}}$. Following a similar approach to the 1-dimensional case, we conclude that stabilization is possible when $f_0c_4>0$ [37].

We now show sample simulation results using the AFHSS method. All the input functions are of the type mentioned in Eq. (30). Figure 10(a) is for *D=2* with the parameters f = [-1,2], Δz = 0.001, M = 8000 A_0 = 1.5, w_0 = 1, L = 0.04 shows the beam evolution. Notice that in this case the beam focuses and defocuses periodically. Figure 10(b) shows the corresponding on-axis amplitude. Figure 11(a) shows the case when *D=3* with the parameters f = [-2,4], Δz= 0.005, M = 7200, A_0 = 1, w_0 = 5, L = 0.015, which leads to a stable soliton. Figure 11(b) shows the corresponding on-axis amplitude.

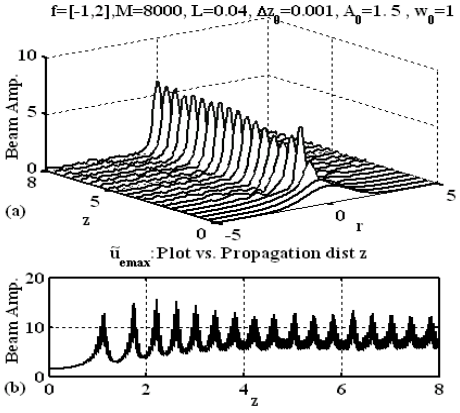

Figure 10. Stable 2-D soliton generation through the sign alternating dispersion using the AFHSS method. (a) pulse evolution. (b) evolution of the on-axis amplitude (Nehmetallah and Banerjee [37]).

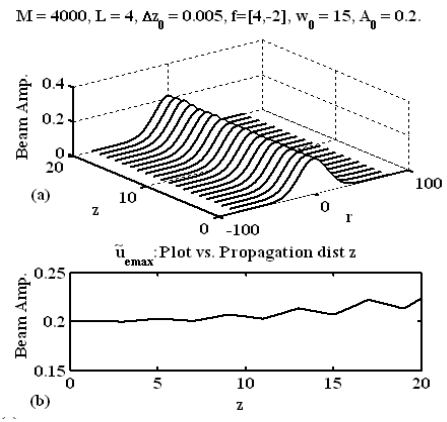

Figure 11. Stable 3-D soliton generation through the sign alternating dispersion, using AFHSS. (a) pulse evolution, (b) evolution of the on-axis amplitude (Nehmetallah and Banerjee [(37]).

7. Nonlinearity management

In this Section we use the same numerical and analytical techniques developed earlier to solve and study transverse and pulsed optical beam or "light bullet" propagation in a layered alternating self-focusing and self-defocusing medium based on the scalar nonlinear Schrödinger (NLS) equation in two and three dimensions with cylindrical and spherical symmetry respectively. It has been shown [23] that a beam can be stabilized if the nonlinearity coefficient is weakly modulated along the propagation direction where the beam power oscillates about the modulated critical value. Moreover, a better stabilization occurs if a more radical modulation of the nonlinearity is done based on a periodically alternating SF and SDF layers, or even periodic SF layers with different values of the Kerr coefficient as shown in [24]. In this case, we have to start from Eq. (19):

$$j\frac{\partial \tilde{u}_e}{\partial z}+\frac{1}{2}\frac{1}{r^{D-1}}\frac{\partial}{\partial r}\left(r^{D-1}\frac{\partial \tilde{u}_e}{\partial r}\right)+g(z)\left|\tilde{u}_e\right|^2\tilde{u}_e=0\cdot \tag{43}$$

A detailed analysis to solve the above equation can be found in Ref. [38].

7.1 The two-dimensional case (D=2)

If we study the stability of Eq. (34d) when $g(z)$ is a harmonic varying function with a dc offset viz., $g(z) = g_0 + g_1 \sin\Omega z$, Eq. (34d) becomes

$$\frac{d^2w}{dz^2} = \frac{-\bar{\varepsilon}_0 + \bar{\varepsilon}\sin\Omega z}{w^3}, \tag{44}$$

where $\bar{\varepsilon}_0 = \frac{-\gamma_1 + N_0\beta_1 g_0}{\alpha_3}$, $\bar{\varepsilon} = \frac{-N_0\beta_1 g_1}{\alpha_3}$. Also, if we make the assumption that the beam radius w can be divided into $w(z) = \tilde{w} + \delta w, \text{with} |\delta w| << |w|$, where $\tilde{w}$ varies on a slow time scale, and δw is a rapidly varying function with a zero mean value, then by means of Kapitza averaging method we derive the following equations from Eq. (44)[39]:

$$\frac{d^2\delta w}{dz^2} = \tilde{w}\bar{\varepsilon}\sin\Omega z + 3\tilde{w}^{-4}\bar{\varepsilon}_0\delta w, \tag{45a}$$

$$\frac{d^2\tilde{w}}{dz^2} = -\tilde{w}^{-3}\bar{\varepsilon}_0 - 6\tilde{w}^{-5}\bar{\varepsilon}_0\langle\delta w^2\rangle - 3\tilde{w}^{-4}\bar{\varepsilon}\langle\delta w\sin\Omega z\rangle, \tag{45b}$$

where $\langle\ldots\rangle$ is the average over the period $2\pi/\Omega$. A particular solution for Eq. (45a) is

$$\delta w(z) = \frac{-\bar{\varepsilon}\sin\Omega z}{\tilde{w}^3\left(\Omega^2 + 3\tilde{w}^{-4}\bar{\varepsilon}_0\right)}, \tag{46}$$

and if we substitute Eq. (46) into Eq. (45b), we obtain the evolution equation of $\tilde{w}$ as

$$\frac{d^2\tilde{w}}{dz^2} = \tilde{w}^{-3}\left[-\bar{\varepsilon}_0 - \frac{3\bar{\varepsilon}_0\bar{\varepsilon}^2}{\left(\Omega^2\tilde{w}^4 + 3\bar{\varepsilon}_0\right)^2} + \frac{3}{2}\frac{\bar{\varepsilon}^2}{\left(\Omega^2\tilde{w}^4 + 3\bar{\varepsilon}_0\right)}\right]. \tag{47}$$

Eq. (47) will have a stable, fixed point solution given by

$$\tilde{w}^4 = \frac{1}{\tilde{\Omega}^2}\left[\frac{3}{4}\frac{\bar{\varepsilon}^2}{\bar{\varepsilon}_0^2}\left(1 + \sqrt{1 - \frac{16}{3}\frac{\bar{\varepsilon}^2}{\bar{\varepsilon}_0^2}}\right) - 3\bar{\varepsilon}_0\right]. \tag{48}$$

Eq. (48) has a real value for the average width $\tilde{w}$ when $\bar{\varepsilon} > \sqrt{6}\bar{\varepsilon}_0$. So for $g_1 < 0$, we must have $g_1 < \sqrt{6}\left(\frac{\gamma_1}{N_0\beta_1} - g_0\right)$, which agrees with the results obtained in [39].

7.2 The three-dimensional case (D=3)

Eq. (34d) becomes

$$\frac{d^2w}{dz^2} = \frac{\tilde{\eta}}{w^3} + \frac{-\hat{\varepsilon}_0 + \hat{\varepsilon}\, sin\,\Omega z}{w^4}, \tag{49}$$

where $\hat{\varepsilon}_0 = \frac{3N_0\beta_2 g_0}{2\alpha_4}$, $\hat{\varepsilon} = \frac{-3N_0\beta_2 g_1}{2\alpha_4}$, and $\tilde{\eta} = \frac{\gamma_2}{\alpha_4}$. Following the same procedure as performed for the two-dimensional case, we get

$$\frac{d^2\delta w}{dz^2} = \left(4\hat{\varepsilon}_0\tilde{w}^{-1} - 3\tilde{\eta}\right)\tilde{w}^{-4}\delta w + \tilde{w}^{-4}\hat{\varepsilon}\, sin\,\Omega z, \tag{50a}$$

$$\frac{d^2\tilde{w}}{dz^2} = \tilde{\eta}\tilde{w}^{-3} - \hat{\varepsilon}_0\tilde{w}^{-4} + \left(6\tilde{\eta}\tilde{w}^{-5} - 10\hat{\varepsilon}_0\tilde{w}\right)\left\langle \delta w^2\right\rangle - 4\tilde{\varepsilon}\tilde{w}^{-5}\left\langle \delta w\, sin\,\Omega z\right\rangle. \tag{50b}$$

A particular solution for Eq. (50a) is

$$\delta w(z) = \frac{-\tilde{w}\hat{\varepsilon}\, sin\,\Omega z}{\tilde{w}^5\Omega^2 - 3\tilde{\eta}\tilde{w} + 4\hat{\varepsilon}_0}. \tag{51}$$

Also, if we substitute Eq. (51) into Eq. (50b), we obtain the evolution equation of $\tilde{w}$ as

$$\frac{d^2\tilde{w}}{dz^2} = \tilde{\eta}\tilde{w}^{-3} - \hat{\varepsilon}_0\tilde{w}^{-4} + \frac{2\hat{\varepsilon}^2\tilde{w}^{-4}}{\tilde{w}^5\Omega^2 - 3\tilde{\eta}\tilde{w} + 4\hat{\varepsilon}_0} + \frac{\tilde{w}^{-4}\hat{\varepsilon}^2\left(3\tilde{\eta}\tilde{w} - 5\hat{\varepsilon}_0\right)}{\left(\tilde{w}^5\Omega^2 - 3\tilde{\eta}\tilde{w} + 4\hat{\varepsilon}_0\right)^2}. \tag{52}$$

Eq. (52) can be written in steady state as

$$\tilde{\eta}\Omega^4\tilde{w}^{11} - \Omega^4\hat{\varepsilon}_0\tilde{w}^{10} + 6\tilde{\eta}^2\Omega^2\tilde{w}^7 - 14\tilde{\eta}\Omega^2\hat{\varepsilon}_0\tilde{w}^6$$

$$+ 2\Omega^2\tilde{w}^5\left(4\hat{\varepsilon}_0^2 + \hat{\varepsilon}^2\right) + 9\tilde{\eta}^3\tilde{w}^3 - 33\tilde{\eta}\hat{\varepsilon}_0\tilde{w}^2$$

$$+ \tilde{\eta}\left(40\hat{\varepsilon}_0^2 - 3\hat{\varepsilon}^2\right)\tilde{w} + 3\hat{\varepsilon}_0\hat{\varepsilon}^2 - 16\hat{\varepsilon}_0^3 = 0. \tag{53}$$

Eq. (53) is solved for the initial conditions $\Delta z = 0.01$, $A_0 = 0.18$, $w_0 = 10$, $g_0 = 1$, $g_1 = -4$, $L_+ = L_- = 0.2$, where one of the steady state real positive roots for the average pulse width $\tilde{w} \approx 10$ which agrees with the initial condition $w_0 = 10$, assumed. Also note that the above equation with the same initial conditions

but with the exception of $\varepsilon_0 < 0$ this time admits no physical solution, which is in agreement with [39].

We now show sample simulation results using the AFHSS method. All the input functions are of the type mentioned in Eq. (30). Figure 12 shows the case for *D=2* with the parameters $\Delta z = 0.01$, $A_0 = 2.1$, $w_0 = 1$, $g_0 = 1$, $g_1 = -2$, $L_+ = L_- = 0.01$. Notice that in these cases the beam focuses and defocuses periodically. Figure 13 shows the case when *D=3* with the following parameters:

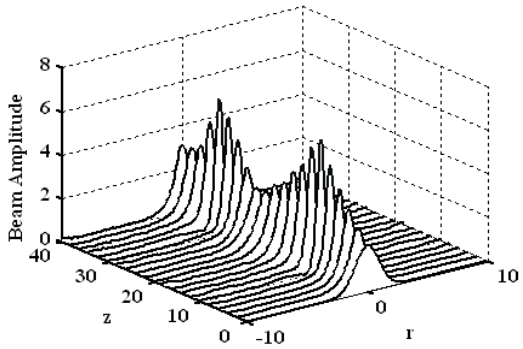

Figure 12. Stable 2-D soliton generation through the sign alternating nonlinearity, using AFHSS with $\widetilde{S} = 2\pi R_1 R_2 = 2\pi \times 800$ (1600 cylindrical samples) (Nehmetallah and Banerjee [38]).

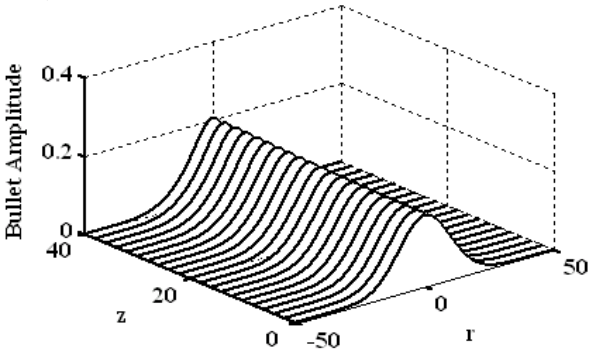

Figure 13. Stable 3-D soliton generation through the sign alternating nonlinearity, using AFHSS with $\widetilde{S} = 2\pi R_1 R_2 = 2\pi \times 800$ (1600 radial samples) (Nehmetallah and Banerjee [38]).

$\Delta z = 0.01$, $A_0 = 0.18$, $w_0 = 10$, $g_0 = 1$, $g_1 = -4$, $L_+ = L_- = 0.2$, which according to the analytical study above leads to a stable soliton, but for ≈ 40 diffraction lengths we see a 10% focusing in the numerical solution [40].

8. Conclusion

In this Chapter, we have provided a brief review of the underlying nonlinear Schrödinger and the Klein-Gordon equation that model spatio-temporal propagation in one and higher dimensions in a nonlinear dispersive environment. While particular analytical solutions are known in certain cases, the vast majority of situations demand numerical solutions. We have summarized a fast adaptive numerical technique based on Hankel transforms to simulate propagation in higher dimensions, as well as referred to other techniques, such as the adaptive wavelet transform method. Nonparaxiality has been treated as an additional term in the NLS equation, and results of stabilization of solitons using nonparaxiality and saturating nonlinearity have been discussed. We have also dealt with dispersion and nonlinearity management in detail, to show how soliton stabilization can be achieved using these techniques. Initial parameters on pulse amplitude, width and nonlinearity and dispersion management parameters required for stable or quasi-stable propagation has to be found using a variational technique, which we have outlined in the Chapter. While dispersion management is widely known, nonlinearity management can be effected through the well-known cascaded quadratic nonlinearities. It is hoped that the numerical methods outlined in the Chapter prove useful for simulation of nonlinear spatio-temporal propagation of optical pulses or optical bullets, in either free-space or in guided wave systems.

References

1. A. Korpel and P.P. Banerjee, "A heuristic guide to nonlinear dispersive wave equations and soliton-type solutions," Proc. IEEE **72** 1109-1130 (1984).
2. N. Zabusky and M. Kruskal, "Interaction of solitons in a collisionless plasma and the recurrence of initial states," Phys. Rev. Lett. **15** 240-243 (1965).
3. R. Dodd, J. Eilbeck, J. Gibbon and H. Morris, *Solitons and Nonlinear Wave Equations*. Academic Press Inc., New York, NY (1982).
4. Y. Kivshar and G. Agrawal, *Optical Solitons*, Academic Press: San Diego, CA (2003).
5. A. Hasegawa and F. Tappert, "Transmission of stationary nonlinear optical pulses in dispersive dielectric fibers. I. Anomalous dispersion," Appl. Phys. Lett. **23** 171-172 (1973).
6. B. A. Malomed, D. Mihalache, F. Wise and L. Torner, "Spatiotemporal optical solitons," J. Opt. B: Quantum Semiclass. Opt. **7** R53- R72 (2005).
7. L. F Mollenauer, R. H Stolen and J.P. Gordon, "Experimental Observation of Picosecond Pulse Narrowing and Solitons in Optical Fibers," Phys. Rev. Lett. **45** 1095-1098 (1980).

8. L. F. Mollenauer and K. Smith, "Demonstration of soliton transmission over more than 4000 km in fiber with loss periodically compensated by Raman gain," Opt. Lett. **13** 675-677 (1988).
9. J. P. Gordon and L. F. Mollenauer, "Effects of fiber nonlinearities and amplifier spacing on ultra-longdistance transmission," J. Lightwave Tech. **9** 170-173 (1991).
10. T. Georges, "Soliton interaction in dispersion-managed links," J. Opt. Soc. Amer. B **15** 1553-1560 (1998).
11. P. Emplit, J. P. Hamaide, F. Reynaud, C. Froehly and A. Barthelemy, "Picosecond steps and dark pulses through nonlinear single mode fibers", Opt. Comm. **62** 374-379 (1987).
12. http://en.wikipedia.org/wiki/Soliton.
13. P.P. Banerjee and T-C. Poon, *Principles of Applied Optics.* Richard D. Irwin, Inc., Homewood, IL (1991).
14. G. Agrawal, *Nonlinear Fiber Optics*. Academic Press, San Diego, CA (1995).
15. R. Chiao, E. Garmire, and C. Townes, "Self-trapping of optical beams," Phys. Rev. Lett. **13** 479-482 (1964).
16. G. Fibich and A. Gaeta, "Critical power for self-focusing in bulk optical media and in hollow waveguides," Opt. Lett. **25** 335-337 (2000).
17. V. E. Zakharov and D. Shabat, "Exact theory of two-dimensional self-focusing and one-dimensional self-modulation of waves in nonlinear media," Sov. Phys.JETP **34** 62-69 (1972).
18. Y. Silberberg, "Collapse of optical pulses," Opt. Lett. **15** 1282-1284 (1990).
19. G. Fibich, "Small Beam Nonparaxiality Arrests Self-Focusing of Optical Beams," Phys. Rev. Lett. **76** 4356-4359 (1996).
20. V. Skarka, V. Berezhiani and R. Miklaszewski, "Spatiotemporal soliton propagation in saturating nonlinear optical media," Phys. Rev. E **56** 1080-1087 (1997).
21. F. Kh. Abdullaev and J. G. Caputo, "Validation of the variational approach for chirped pulses in fibers with periodic dispersion," Phys. Rev. E **58** 6637-6648 (1998).
22. F. Kh. Abdullaev, B. B. Baizakov and M. Salerno, "Stable two-dimensional dispersion-managed soliton," Phys. Rev. E **68,** 066605-1-066605-4 (2003).
23. L. Berge, V.K. Mezentsev, J. Juul Rasmussen, P.L. Christiansen and Yu. B. Gaididei, "Self-guiding light in layered nonlinear media," Opt. Lett. **25** 1037-1039 (2000).
24. I. Towers and B. A. Malomed, "Stable (2+1)-dimensional solitons in a layered medium with sign-alternating Kerr nonlinearity," J. Opt. Soc. Amer. B **19** 537-543 (2002).
25. G. I. Stegeman, M. Sheik-Bahae, E. W. Van Stryland and G. Assanto, "Large nonlinear phase shifts in second-order nonlinear-optical processes," Opt. Lett. **18** 13-15 (1993).
26. A. Siegman, "Quasi-fast Hankel transform," Opt. Lett. **1** 13-15 (1977).
27. V. Magni, G. Cerullo, and S. De Silvestri, "High-accuracy fast Hankel transform for optical beam propagation," J. Opt. Soc. Amer. A **9** 2031-2033 (1992).
28. L. Yu, M. Huang, M. Chen, W. Chen, W. Huang and Z. Zhu, "Quasi-discrete Hankel transform," Opt. Lett. **23** 409-411 (1998).

29. M. Guizar-Sicairos and J. Gutiérrez-Vega, “Computation of quasi-discrete Hankel transform of integer order for propagating optical wave fields”, J. Opt. Soc. Amer. A **21** 53-58 (2004).
30. I. Sneddon, *The Use of Integral Transform*, McGraw-Hill, New York, NY (1972).
31. P. P. Banerjee, G. Nehmetallah and M. Chatterjee, “Numerical Modeling of Cylindrically Symmetric Nonlinear Self-focusing Using an Adaptive Fast Hankel Split-step Method,” Opt. Comm. **249** 293-300 (2005).
32. G. Fibich and B. Ilan, “Discretization effects in the nonlinear Schrödinger equation,” App. Num. Math. **44** 63-75 (2003).
33. G. Nehmetallah and P. P. Banerjee, “Numerical Modeling of Spatiotemporal Solitons Using an Adaptive Spherical Fourier Bessel Split Step Method,” Opt. Comm. **257** 197-205 (2006).
34. M. Stedham and P. P. Banerjee, ”Detailed resolution of the nonlinear Schrödinger equation using the full adaptive wavelet transform,” Proc. SPIE **4056** 24-28 (2000).
35. M. Desaix, D. Anderson, and M. Lisak, “Variational approach to collapse of optical pulses,” J. Opt. Soc. Amer. B **8** 2082-2086 (1991).
36. G. Nehmetallah, and P. P. Banerjee, “Stabilization of a (D+1)-dimensional Dispersion Managed Solitons in Kerr Media by an Alternating Dispersion Structure,” J. Opt. Soc. Amer. B **23** 203-211 (2006).
37. G. Nehmetallah and P.P. Banerjee, “Analysis of Spatial and Spatio-temporal Soliton Propagation Using a Fast Adaptive Fourier-Bessel Transform Technique,” Proc. Int. Conf. on Opt. and Optoelectronics, India, IT-NLO 1, Dec. (2005).
38. G. Nehmetallah and P. P. Banerjee, “Numerical Modeling of (D+1)-dimensional Solitons in a Sign Alternating Nonlinear Medium Using an Adaptive Fast Hankel Split Step Method,” J. Opt. Soc. Amer. B **22** 2200-2207 (2005).
39. F. K. Abdullaev, J. G. Caputo, R.A. Kraenkel and B.A. Malomed, “Controlling collapse in Bose-Einstein condensates by temporal modulation of the scattering length,” Phys. Rev. A **67** 013605 (2003).
40. G. Nehmetallah and P.P. Banerjee, “An Adaptive Spherical Fourier Bessel Split-step Method for Tracking Optical Bullets,” Proc. SPIE Int. Soc. Opt. Eng. **5892** 589217.1-589217.12 (2005).